Exclusive initial-state-radiation production of the $D\bar{D}$, $D^*\bar{D}$, and $D^*\bar{D}^*$ systems

B. Aubert,[1] Y. Karyotakis,[1] J. P. Lees,[1] V. Poireau,[1] E. Prencipe,[1] X. Prudent,[1] V. Tisserand,[1] J. Garra Tico,[2] E. Grauges,[2] L. Lopez,[3a,3b] A. Palano,[3a,3b] M. Pappagallo,[3a,3b] G. Eigen,[4] B. Stugu,[4] L. Sun,[4] M. Battaglia,[5] D. N. Brown,[5] L. T. Kerth,[5] Yu. G. Kolomensky,[5] G. Lynch,[5] I. L. Osipenkov,[5] K. Tackmann,[5] T. Tanabe,[5] C. M. Hawkes,[6] N. Soni,[6] A. T. Watson,[6] H. Koch,[7] T. Schroeder,[7] D. J. Asgeirsson,[8] B. G. Fulsom,[8] C. Hearty,[8] T. S. Mattison,[8] J. A. McKenna,[8] M. Barrett,[9] A. Khan,[9] A. Randle-Conde,[9] V. E. Blinov,[10] A. D. Bukin,[10] A. R. Buzykaev,[10] V. P. Druzhinin,[10] V. B. Golubev,[10] A. P. Onuchin,[10] S. I. Serednyakov,[10] Yu. I. Skovpen,[10] E. P. Solodov,[10] K. Yu. Todyshev,[10] M. Bondioli,[11] S. Curry,[11] I. Eschrich,[11] D. Kirkby,[11] A. J. Lankford,[11] P. Lund,[11] M. Mandelkern,[11] E. C. Martin,[11] D. P. Stoker,[11] S. Abachi,[12] C. Buchanan,[12] H. Atmacan,[13] J. W. Gary,[13] F. Liu,[13] O. Long,[13] G. M. Vitug,[13] Z. Yasin,[13] L. Zhang,[13] V. Sharma,[14] C. Campagnari,[15] T. M. Hong,[15] D. Kovalskyi,[15] M. A. Mazur,[15] J. D. Richman,[15] T. W. Beck,[16] A. M. Eisner,[16] C. A. Heusch,[16] J. Kroseberg,[16] W. S. Lockman,[16] A. J. Martinez,[16] T. Schalk,[16] B. A. Schumm,[16] A. Seiden,[16] L. O. Winstrom,[16] C. H. Cheng,[17] D. A. Doll,[17] B. Echenard,[17] F. Fang,[17] D. G. Hitlin,[17] I. Narsky,[17] T. Piatenko,[17] F. C. Porter,[17] R. Andreassen,[18] G. Mancinelli,[18] B. T. Meadows,[18] K. Mishra,[18] M. D. Sokoloff,[18] P. C. Bloom,[19] W. T. Ford,[19] A. Gaz,[19] J. F. Hirschauer,[19] M. Nagel,[19] U. Nauenberg,[19] J. G. Smith,[19] S. R. Wagner,[19] R. Ayad,[20,*] A. Soffer,[20,†] W. H. Toki,[20] R. J. Wilson,[20] E. Feltresi,[21] A. Hauke,[21] H. Jasper,[21] M. Karbach,[21] J. Merkel,[21] A. Petzold,[21] B. Spaan,[21] K. Wacker,[21] M. J. Kobel,[22] R. Nogowski,[22] K. R. Schubert,[22] R. Schwierz,[22] A. Volk,[22] D. Bernard,[23] G. R. Bonneaud,[23] E. Latour,[23] M. Verderi,[23] P. J. Clark,[24] S. Playfer,[24] J. E. Watson,[24] M. Andreotti,[25a,25b] D. Bettoni,[25a] C. Bozzi,[25a] R. Calabrese,[25a,25b] A. Cecchi,[25a,25b] G. Cibinetto,[25a,25b] P. Franchini,[25a,25b] E. Luppi,[25a,25b] M. Negrini,[25a,25b] A. Petrella,[25a,25b] L. Piemontese,[25a] V. Santoro,[25a,25b] R. Baldini-Ferroli,[26] A. Calcaterra,[26] R. de Sangro,[26] G. Finocchiaro,[26] S. Pacetti,[26] P. Patteri,[26] I. M. Peruzzi,[26,‡] M. Piccolo,[26] M. Rama,[26] A. Zallo,[26] R. Contri,[27a,27b] E. Guido, M. Lo Vetere,[27a,27b] M. R. Monge,[27a,27b] S. Passaggio,[27a] C. Patrignani,[27a,27b] E. Robutti,[27a] S. Tosi,[27a,27b] K. S. Chaisanguanthum,[28] M. Morii,[28] A. Adametz,[29] J. Marks,[29] S. Schenk,[29] U. Uwer,[29] F. U. Bernlochner,[30] V. Klose,[30] H. M. Lacker,[30] D. J. Bard,[31] P. D. Dauncey,[31] M. Tibbetts,[31] P. K. Behera,[32] X. Chai,[32] M. J. Charles,[32] U. Mallik,[32] J. Cochran,[33] H. B. Crawley,[33] L. Dong,[33] W. T. Meyer,[33] S. Prell,[33] E. I. Rosenberg,[33] A. E. Rubin,[33] Y. Y. Gao,[34] A. V. Gritsan,[34] Z. J. Guo,[34] N. Arnaud,[35] J. Béquilleux,[35] A. D'Orazio,[35] M. Davier,[35] J. Firmino da Costa,[35] G. Grosdidier,[35] F. Le Diberder,[35] V. Lepeltier,[35] A. M. Lutz,[35] S. Pruvot,[35] P. Roudeau,[35] M. H. Schune,[35] J. Serrano,[35] V. Sordini,[35,§] A. Stocchi,[35] G. Wormser,[35] D. J. Lange,[36] D. M. Wright,[36] I. Bingham,[37] J. P. Burke,[37] C. A. Chavez,[37] J. R. Fry,[37] E. Gabathuler,[37] R. Gamet,[37] D. E. Hutchcroft,[37] D. J. Payne,[37] C. Touramanis,[37] A. J. Bevan,[38] C. K. Clarke,[38] F. Di Lodovico,[38] R. Sacco,[38] M. Sigamani,[38] G. Cowan,[39] S. Paramesvaran,[39] A. C. Wren,[39] D. N. Brown,[40] C. L. Davis,[40] A. G. Denig,[41] M. Fritsch,[41] W. Gradl,[41] A. Hafner,[41] K. E. Alwyn,[42] D. Bailey,[42] R. J. Barlow,[42] G. Jackson,[42] G. D. Lafferty,[42] T. J. West,[42] J. I. Yi,[42] J. Anderson,[43] C. Chen,[43] A. Jawahery,[43] D. A. Roberts,[43] G. Simi,[43] J. M. Tuggle,[43] C. Dallapiccola,[44] E. Salvati,[44] S. Saremi,[44] R. Cowan,[45] D. Dujmic,[45] P. H. Fisher,[45] S. W. Henderson,[45] G. Sciolla,[45] M. Spitznagel,[45] R. K. Yamamoto,[45] M. Zhao,[45] P. M. Patel,[46] S. H. Robertson,[46] M. Schram,[46] A. Lazzaro,[47a,47b] V. Lombardo,[47a] F. Palombo,[47a,47b] S. Stracka, J. M. Bauer,[48] L. Cremaldi,[48] R. Godang,[48,‖] R. Kroeger,[48] D. J. Summers,[48] H. W. Zhao,[48] M. Simard,[49] P. Taras,[49] H. Nicholson,[50] G. De Nardo,[51a,51b] L. Lista,[51a] D. Monorchio,[51a,51b] G. Onorato,[51a,51b] C. Sciacca,[51a,51b] G. Raven,[52] H. L. Snoek,[52] C. P. Jessop,[53] K. J. Knoepfel,[53] J. M. LoSecco,[53] W. F. Wang,[53] L. A. Corwin,[54] K. Honscheid,[54] H. Kagan,[54] R. Kass,[54] J. P. Morris,[54] A. M. Rahimi,[54] J. J. Regensburger,[54] S. J. Sekula,[54] Q. K. Wong,[54] N. L. Blount,[55] J. Brau,[55] R. Frey,[55] O. Igonkina,[55] J. A. Kolb,[55] M. Lu,[55] R. Rahmat,[55] N. B. Sinev,[55] D. Strom,[55] J. Strube,[55] E. Torrence,[55] G. Castelli,[56a,56b] N. Gagliardi,[56a,56b] M. Margoni,[56a,56b] M. Morandin,[56a] M. Posocco,[56a] M. Rotondo,[56a] F. Simonetto,[56a,56b] R. Stroili,[56a,56b] C. Voci,[56a,56b] P. del Amo Sanchez,[57] E. Ben-Haim,[57] H. Briand,[57] J. Chauveau,[57] O. Hamon,[57] Ph. Leruste,[57] J. Ocariz,[57] A. Perez,[57] J. Prendki,[57] S. Sitt,[57] L. Gladney,[58] M. Biasini,[59a,59b] E. Manoni,[59a,59b] C. Angelini,[60a,60b] G. Batignani,[60a,60b] S. Bettarini,[60a,60b] G. Calderini,[60a,60b,¶] M. Carpinelli,[60a,60b,**] A. Cervelli,[60a,60b] F. Forti,[60a,60b] M. A. Giorgi,[60a,60b] A. Lusiani,[60a,60c] G. Marchiori,[60a,60b] M. Morganti,[60a,60b] N. Neri,[60a,60b] E. Paoloni,[60a,60b] G. Rizzo,[60a,60b] J. J. Walsh,[60a] D. Lopes Pegna,[61] C. Lu,[61] J. Olsen,[61] A. J. S. Smith,[61] A. V. Telnov,[61] F. Anulli,[62a] E. Baracchini,[62a,62b] G. Cavoto,[62a] R. Faccini,[62a,62b] F. Ferrarotto,[62a] F. Ferroni,[62a,62b] M. Gaspero,[62a,62b] P. D. Jackson,[62a] L. Li Gioi,[62a] M. A. Mazzoni,[62a] S. Morganti,[62a] G. Piredda,[62a] F. Renga,[62a,62b] C. Voena,[62a] M. Ebert,[63] T. Hartmann,[63] H. Schröder,[63] R. Waldi,[63] T. Adye,[64] B. Franek,[64] E. O. Olaiya,[64] F. F. Wilson,[64] S. Emery,[65] L. Esteve,[65] G. Hamel de Monchenault,[65] W. Kozanecki,[65] G. Vasseur,[65] Ch. Yèche,[65] M. Zito,[65] X. R. Chen,[66] H. Liu,[66] W. Park,[66] M. V. Purohit,[66] R. M. White,[66] J. R. Wilson,[66] M. T. Allen,[67] D. Aston,[67] R. Bartoldus,[67] J. F. Benitez,[67] R. Cenci,[67] J. P. Coleman,[67] M. R. Convery,[67] J. C. Dingfelder,[67] J. Dorfan,[67]

G. P. Dubois-Felsmann,[67] W. Dunwoodie,[67] R. C. Field,[67] A. M. Gabareen,[67] M. T. Graham,[67] P. Grenier,[67] C. Hast,[67] W. R. Innes,[67] J. Kaminski,[67] M. H. Kelsey,[67] H. Kim,[67] P. Kim,[67] M. L. Kocian,[67] D. W. G. S. Leith,[67] S. Li,[67] B. Lindquist,[67] S. Luitz,[67] V. Luth,[67] H. L. Lynch,[67] D. B. MacFarlane,[67] H. Marsiske,[67] R. Messner,[67] D. R. Muller,[67] H. Neal,[67] S. Nelson,[67] C. P. O'Grady,[67] I. Ofte,[67] M. Perl,[67] B. N. Ratcliff,[67] A. Roodman,[67] A. A. Salnikov,[67] R. H. Schindler,[67] J. Schwiening,[67] A. Snyder,[67] D. Su,[67] M. K. Sullivan,[67] K. Suzuki,[67] S. K. Swain,[67] J. M. Thompson,[67] J. Va'vra,[67] A. P. Wagner,[67] M. Weaver,[67] C. A. West,[67] W. J. Wisniewski,[67] M. Wittgen,[67] D. H. Wright,[67] H. W. Wulsin,[67] A. K. Yarritu,[67] K. Yi,[67] C. C. Young,[67] V. Ziegler,[67] P. R. Burchat,[68] A. J. Edwards,[68] T. S. Miyashita,[68] S. Ahmed,[69] M. S. Alam,[69] J. A. Ernst,[69] B. Pan,[69] M. A. Saeed,[69] S. B. Zain,[69] S. M. Spanier,[70] B. J. Wogsland,[70] R. Eckmann,[71] J. L. Ritchie,[71] A. M. Ruland,[71] C. J. Schilling,[71] R. F. Schwitters,[71] B. W. Drummond,[72] J. M. Izen,[72] X. C. Lou,[72] F. Bianchi,[73a,73b] D. Gamba,[73a,73b] M. Pelliccioni,[73a,73b] M. Bomben,[74a,74b] L. Bosisio,[74a,74b] C. Cartaro,[74a,74b] G. Della Ricca,[74a,74b] L. Lanceri,[74a,74b] L. Vitale,[74a,74b] V. Azzolini,[75] N. Lopez-March,[75] F. Martinez-Vidal,[75] D. A. Milanes,[75] A. Oyanguren,[75] J. Albert,[76] Sw. Banerjee,[76] B. Bhuyan,[76] H. H. F. Choi,[76] K. Hamano,[76] G. J. King,[76] R. Kowalewski,[76] M. J. Lewczuk,[76] I. M. Nugent,[76] J. M. Roney,[76] R. J. Sobie,[76] T. J. Gershon,[77] P. F. Harrison,[77] J. Ilic,[77] T. E. Latham,[77] G. B. Mohanty,[77] E. M. T. Puccio,[77] H. R. Band,[78] X. Chen,[78] S. Dasu,[78] K. T. Flood,[78] Y. Pan,[78] R. Prepost,[78] C. O. Vuosalo,[78] and S. L. Wu[78]

(*BABAR* Collaboration)

[1]*Laboratoire d'Annecy-le-Vieux de Physique des Particules (LAPP), Université de Savoie, CNRS/IN_2P_3, F-74941 Annecy-Le-Vieux, France*
[2]*Universitat de Barcelona, Facultat de Fisica, Departament ECM, E-08028 Barcelona, Spain*
[3a]*INFN Sezione di Bari, I-70126 Bari, Italy*
[3b]*Dipartimento di Fisica, Università di Bari, I-70126 Bari, Italy*
[4]*University of Bergen, Institute of Physics, N-5007 Bergen, Norway*
[5]*Lawrence Berkeley National Laboratory and University of California, Berkeley, California 94720, USA*
[6]*University of Birmingham, Birmingham, B15 2TT, United Kingdom*
[7]*Ruhr Universität Bochum, Institut für Experimentalphysik 1, D-44780 Bochum, Germany*
[8]*University of British Columbia, Vancouver, British Columbia, Canada V6T 1Z1*
[9]*Brunel University, Uxbridge, Middlesex UB8 3PH, United Kingdom*
[10]*Budker Institute of Nuclear Physics, Novosibirsk 630090, Russia*
[11]*University of California at Irvine, Irvine, California 92697, USA*
[12]*University of California at Los Angeles, Los Angeles, California 90024, USA*
[13]*University of California at Riverside, Riverside, California 92521, USA*
[14]*University of California at San Diego, La Jolla, California 92093, USA*
[15]*University of California at Santa Barbara, Santa Barbara, California 93106, USA*
[16]*University of California at Santa Cruz, Institute for Particle Physics, Santa Cruz, California 95064, USA*
[17]*California Institute of Technology, Pasadena, California 91125, USA*
[18]*University of Cincinnati, Cincinnati, Ohio 45221, USA*
[19]*University of Colorado, Boulder, Colorado 80309, USA*
[20]*Colorado State University, Fort Collins, Colorado 80523, USA*
[21]*Technische Universität Dortmund, Fakultät Physik, D-44221 Dortmund, Germany*
[22]*Technische Universität Dresden, Institut für Kern- und Teilchenphysik, D-01062 Dresden, Germany*
[23]*Laboratoire Leprince-Ringuet, CNRS/IN_2P_3, Ecole Polytechnique, F-91128 Palaiseau, France*
[24]*University of Edinburgh, Edinburgh EH9 3JZ, United Kingdom*
[25a]*INFN Sezione di Ferrara, I-44100 Ferrara, Italy*
[25b]*Dipartimento di Fisica, Università di Ferrara, I-44100 Ferrara, Italy*
[26]*INFN Laboratori Nazionali di Frascati, I-00044 Frascati, Italy*
[27a]*INFN Sezione di Genova, I-16146 Genova, Italy*
[27b]*Dipartimento di Fisica, Università di Genova, I-16146 Genova, Italy*
[28]*Harvard University, Cambridge, Massachusetts 02138, USA*
[29]*Universität Heidelberg, Physikalisches Institut, Philosophenweg 12, D-69120 Heidelberg, Germany*
[30]*Humboldt-Universität zu Berlin, Institut für Physik, Newtonstr. 15, D-12489 Berlin, Germany*
[31]*Imperial College London, London, SW7 2AZ, United Kingdom*
[32]*University of Iowa, Iowa City, Iowa 52242, USA*
[33]*Iowa State University, Ames, Iowa 50011-3160, USA*
[34]*Johns Hopkins University, Baltimore, Maryland 21218, USA*
[35]*Laboratoire de l'Accélérateur Linéaire, IN_2P_3/CNRS et Université Paris-Sud 11, Centre Scientifique d'Orsay, B. P. 34, F-91898 Orsay Cedex, France*

[36]*Lawrence Livermore National Laboratory, Livermore, California 94550, USA*
[37]*University of Liverpool, Liverpool L69 7ZE, United Kingdom*
[38]*Queen Mary, University of London, London, E1 4NS, United Kingdom*
[39]*University of London, Royal Holloway and Bedford New College, Egham, Surrey TW20 0EX, United Kingdom*
[40]*University of Louisville, Louisville, Kentucky 40292, USA*
[41]*Johannes Gutenberg-Universität Mainz, Institut für Kernphysik, D-55099 Mainz, Germany*
[42]*University of Manchester, Manchester M13 9PL, United Kingdom*
[43]*University of Maryland, College Park, Maryland 20742, USA*
[44]*University of Massachusetts, Amherst, Massachusetts 01003, USA*
[45]*Massachusetts Institute of Technology, Laboratory for Nuclear Science, Cambridge, Massachusetts 02139, USA*
[46]*McGill University, Montréal, Québec, Canada H3A 2T8*
[47a]*INFN Sezione di Milano, I-20133 Milano, Italy*
[47b]*Dipartimento di Fisica, Università di Milano, I-20133 Milano, Italy*
[48]*University of Mississippi, University, Mississippi 38677, USA*
[49]*Université de Montréal, Physique des Particules, Montréal, Québec, Canada H3C 3J7*
[50]*Mount Holyoke College, South Hadley, Massachusetts 01075, USA*
[51a]*INFN Sezione di Napoli, I-80126 Napoli, Italy*
[51b]*Dipartimento di Scienze Fisiche, Università di Napoli Federico II, I-80126 Napoli, Italy*
[52]*NIKHEF, National Institute for Nuclear Physics and High Energy Physics, NL-1009 DB Amsterdam, The Netherlands*
[53]*University of Notre Dame, Notre Dame, Indiana 46556, USA*
[54]*Ohio State University, Columbus, Ohio 43210, USA*
[55]*University of Oregon, Eugene, Oregon 97403, USA*
[56a]*INFN Sezione di Padova, I-35131 Padova, Italy*
[56b]*Dipartimento di Fisica, Università di Padova, I-35131 Padova, Italy*
[57]*Laboratoire de Physique Nucléaire et de Hautes Energies, IN_2P_3/CNRS, Université Pierre et Marie Curie-Paris6, Université Denis Diderot-Paris7, F-75252 Paris, France*
[58]*University of Pennsylvania, Philadelphia, Pennsylvania 19104, USA*
[59a]*INFN Sezione di Perugia, I-06100 Perugia, Italy*
[59b]*Dipartimento di Fisica, Università di Perugia, I-06100 Perugia, Italy*
[60a]*INFN Sezione di Pisa, I-56127 Pisa, Italy*
[60b]*Dipartimento di Fisica, Università di Pisa, I-56127 Pisa, Italy*
[60c]*Scuola Normale Superiore di Pisa, I-56127 Pisa, Italy*
[61]*Princeton University, Princeton, New Jersey 08544, USA*
[62a]*INFN Sezione di Roma, I-00185 Roma, Italy*
[62b]*Dipartimento di Fisica, Università di Roma La Sapienza, I-00185 Roma, Italy*
[63]*Universität Rostock, D-18051 Rostock, Germany*
[64]*Rutherford Appleton Laboratory, Chilton, Didcot, Oxon, OX11 0QX, United Kingdom*
[65]*CEA, Irfu, SPP, Centre de Saclay, F-91191 Gif-sur-Yvette, France*
[66]*University of South Carolina, Columbia, South Carolina 29208, USA*
[67]*SLAC National Accelerator Laboratory, Stanford, California 94309, USA*
[68]*Stanford University, Stanford, California 94305-4060, USA*
[69]*State University of New York, Albany, New York 12222, USA*
[70]*University of Tennessee, Knoxville, Tennessee 37996, USA*
[71]*University of Texas at Austin, Austin, Texas 78712, USA*
[72]*University of Texas at Dallas, Richardson, Texas 75083, USA*
[73a]*INFN Sezione di Torino, I-10125 Torino, Italy*
[73b]*Dipartimento di Fisica Sperimentale, Università di Torino, I-10125 Torino, Italy*
[74a]*INFN Sezione di Trieste, I-34127 Trieste, Italy*
[74b]*Dipartimento di Fisica, Università di Trieste, I-34127 Trieste, Italy*
[75]*IFIC, Universitat de Valencia-CSIC, E-46071 Valencia, Spain*

[*]Now at Temple University, Philadelphia, PA 19122, USA
[†]Now at Tel Aviv University, Tel Aviv, 69978, Israel
[‡]Also with Università di Perugia, Dipartimento di Fisica, Perugia, Italy
[§]Also with Università di Roma La Sapienza, I-00185 Roma, Italy
[‖]Now at University of South Alabama, Mobile, AL 36688, USA
[¶]Also with Laboratoire de Physique Nucléaire et de Hautes Energies, IN_2P_3/CNRS, Université Pierre et Marie Curie-Paris6, Université Denis Diderot-Paris7, F-75252 Paris, France
[**]Also with Università di Sassari, Sassari, Italy

[76]*University of Victoria, Victoria, British Columbia, Canada V8W 3P6*
[77]*Department of Physics, University of Warwick, Coventry CV4 7AL, United Kingdom*
[78]*University of Wisconsin, Madison, Wisconsin 53706, USA*

(Received 9 March 2009; published 5 May 2009; publisher error corrected 21 July 2009)

We perform a study of the exclusive production of $D\bar{D}$, $D^*\bar{D}$, and $D^*\bar{D}^*$ in initial-state-radiation events, from e^+e^- annihilations at a center-of-mass energy near 10.58 GeV, to search for charmonium and possible new resonances. The data sample corresponds to an integrated luminosity of 384 fb^{-1} and was recorded by the *BABAR* experiment at the PEP-II storage rings. The $D\bar{D}$, $D^*\bar{D}$, and $D^*\bar{D}^*$ mass spectra show clear evidence of several ψ resonances. However, there is no evidence for $Y(4260) \to D^*\bar{D}$ or $Y(4260) \to D^*\bar{D}^*$.

DOI: 10.1103/PhysRevD.79.092001 PACS numbers: 13.66.Bc, 13.87.Fh, 14.40.Gx

I. INTRODUCTION

The surprising discovery of new states decaying to $J/\psi\pi^+\pi^-$ [1,2] has renewed interest in the field of charmonium spectroscopy, since the new resonances are not easy to accommodate in the quark model. In particular, the *BABAR* experiment discovered a new broad state $Y(4260)$, decaying to $J/\psi\pi^+\pi^-$ in the initial-state-radiation (ISR) reaction $e^+e^- \to \gamma_{\rm ISR}Y(4260)$. The quantum numbers $J^{PC} = 1^{--}$ are inferred from the single virtual-photon production mechanism. Further structures at 4.36 GeV/c^2 [3,4] and 4.66 GeV/c^2 [4] have been observed in the $\psi(2S)\pi^+\pi^-$ mass distribution from the reaction $e^+e^- \to \gamma_{\rm ISR}\psi(2S)\pi^+\pi^-$. Charmonium states at these masses would be expected [5,6] to decay predominantly to $D\bar{D}$, $D^*\bar{D}$, or $D^*\bar{D}^*$ [7]. It is peculiar that the decay rate to the hidden charm final state $J/\psi\pi^+\pi^-$ is much larger for the $Y(4260)$ than for excited charmonium states [8], and that at the $Y(4260)$ mass the cross section for $e^+e^- \to$ hadrons exhibits a local minimum [9]. Several theoretical interpretations for the $Y(4260)$ have been proposed, including unconventional scenarios: quark-antiquark gluon hybrids [10], baryonium [11], tetraquarks [12], and hadronic molecules [13]. For a discussion and a list of references see, for example, Ref. [14].

This work explores ISR production of $D\bar{D}$, $D^*\bar{D}$, and $D^*\bar{D}^*$ final states for evidence of charmonium states and unconventional structures. This follows an earlier *BABAR* measurement of the $D\bar{D}$ cross section [15]. A study by the Belle Collaboration of the $D\bar{D}$, $D^*\bar{D}$, and $D^*\bar{D}^*$ final states can be found in Refs. [16,17]. Recent measurements of the e^+e^- cross sections can be found in Ref. [18].

We also measure for the first time branching fractions of high mass charmonium states, other than $Y(4260)$, for which little information exists [9], and compare our measurements with theoretical expectations [5,6,14].

This paper is organized as follows: In Sec. II, we give a short description of the *BABAR* experiment, and in Sec. III, we describe the data selection. Section IV is devoted to the selection of the $D^*\bar{D}$ final state, and in Sec. V, we present the mass resolution, reconstruction efficiency, and measured cross sections. In Sec. VI, we describe the $D^*\bar{D}^*$ cross section measurement, while in Sec. VII, we present the $D\bar{D}$ data. The description of the fit of the three channels is described in Sec. VIII, while Sec. IX is devoted to the measurements of the ratios of branching fractions. Finally, in Section X, we compute the limit on production of $Y(4260)$ decaying to $D^*\bar{D}$ and $D^*\bar{D}^*$, and summarize conclusions in Sec. XI.

II. THE *BABAR* EXPERIMENT

This analysis is based on a 384 fb^{-1} data sample recorded at the $\Upsilon(4S)$ resonance and 40 MeV below the resonance by the *BABAR* detector at the PEP-II asymmetric-energy e^+e^- storage rings. The *BABAR* detector is described in detail elsewhere [19]. We mention here only the parts of the detector that are used in the present analysis. Charged particles are detected and their momenta measured with a combination of a cylindrical drift chamber and a silicon vertex tracker, both operating within a 1.5 T magnetic field of a superconducting solenoid. The information from a ring-imaging Cherenkov detector combined with energy-loss measurements in the silicon vertex tracker and drift chamber provide identification of charged kaon and pion candidates. Photon energies are measured with a CsI(Tl) electromagnetic calorimeter.

III. DATA SELECTION

$D\bar{D}$ candidates are reconstructed in the seven final states listed in Table I.

The $D^{*0} \to D^0\pi^0$ and $D^{*0} \to D^0\gamma$ decay modes are used to form $D^{*0}\bar{D}^0$ and $D^{*0}\bar{D}^{*0}$ candidates. The $D^{*+} \to D^0\pi^+$ and $D^{*+} \to D^+\pi^0$ decay modes are used to form

TABLE I. List of the reconstructed $D\bar{D}$ final states.

N	Channel	First D decay mode	Second D decay mode
1	$D^0\bar{D}^0$	$D^0 \to K^-\pi^+$	$\bar{D}^0 \to K^+\pi^-$
2	$D^0\bar{D}^0$	$D^0 \to K^-\pi^+$	$\bar{D}^0 \to K^+\pi^-\pi^0$
3	$D^0\bar{D}^0$	$D^0 \to K^-\pi^+$	$\bar{D}^0 \to K^+\pi^-\pi^+\pi^-$
4	$D^0\bar{D}^0$	$D^0 \to K^-\pi^+\pi^0$	$\bar{D}^0 \to K^+\pi^-\pi^+\pi^-$
5	D^+D^-	$D^+ \to K^-\pi^+\pi^+$	$D^- \to K^+\pi^-\pi^-$
6	D^+D^-	$D^+ \to K^-\pi^+\pi^+$	$D^- \to K^+K^-\pi^-$
7	D^+D^-	$D^+ \to K^-\pi^+\pi^+$	$D^- \to K^0_S\pi^-$

TABLE II. List of the $D^*\bar{D}$ and $D^*\bar{D}^*$ reconstructed final states. The reconstructed D^0 decay modes are listed in Table I for the $D^{*0}\bar{D}$ and $D^{*0}\bar{D}^{*0}$ states. The column headed Veto lists ambiguities with the indicated channels, "Removed" indicates the fraction of events removed by the Veto.

N	Channel	First decay mode	Second decay mode	Veto	Removed %
8	$D^{*0}\bar{D}^0$	$D^{*0} \to D^0\gamma$		9–12	5.9
9	$D^{*0}\bar{D}^0$	$D^{*0} \to D^0\pi^0$		11,12	3.2
10	$D^{*0}\bar{D}^{*0}$	$D^{*0} \to D^0\gamma$	$\bar{D}^{*0} \to \bar{D}^0\gamma$	9,11	1.1
11	$D^{*0}\bar{D}^{*0}$	$D^{*0} \to D^0\pi^0$	$\bar{D}^{*0} \to \bar{D}^0\gamma$	8,10	0.7
12	$D^{*0}\bar{D}^{*0}$	$D^{*0} \to D^0\pi^0$	$\bar{D}^{*0} \to \bar{D}^0\pi^0$		
13	$D^{*+}D^-$	$D^{*+} \to D^0\pi^+$, $D^0 \to K^-\pi^+$	$D^- \to K^+\pi^-\pi^-$		
14	$D^{*+}D^-$	$D^{*+} \to D^+\pi^0$, $D^+ \to K^-\pi^+\pi^+$	$D^- \to K^+\pi^-\pi^-$		
15	$D^{*+}D^-$	$D^{*+} \to D^0\pi^+$, $D^0 \to K^-K^+$	$D^- \to K^+\pi^-\pi^-$		
16	$D^{*+}D^-$	$D^{*+} \to D^0\pi^+$, $D^0 \to K^-\pi^+$	$D^- \to K^+K^-\pi^-$		
17	$D^{*+}D^-$	$D^{*+} \to D^+\pi^0$, $D^+ \to K^-\pi^+\pi^+$	$D^- \to K^+K^-\pi^-$		
18	$D^{*+}D^{*-}$	$D^{*+} \to D^0\pi^+$, $D^0 \to K^-\pi^+$	$D^{*-} \to \bar{D}^0\pi^-$, $\bar{D}^0 \to K^+\pi^-$		
19	$D^{*+}D^{*-}$	$D^{*+} \to D^+\pi^0$, $D^+ \to K^-\pi^+\pi^+$	$D^{*-} \to \bar{D}^0\pi^-$, $\bar{D}^0 \to K^+\pi^-$		

$D^{*+}D^-$ and $D^{*+}D^{*-}$ candidates. Table II summarizes the full decay chains used to reconstruct the $D^*\bar{D}$ and $D^*\bar{D}^*$ candidates.

For all final states, events are retained if the number of well-measured charged tracks, having a minimum transverse momentum of 0.1 GeV/c, is exactly equal to the total number of charged daughter particles. Photons are identified as electromagnetic clusters that do not have a spatial match with a charged track, and that have a minimum energy of 30 MeV. Neutral pion candidates are formed from pairs of photons kinematically fitted with the π^0 mass constraint. K^0_S candidates are reconstructed, with a vertex fit, in the $\pi^+\pi^-$ decay mode. The tracks corresponding to the charged daughters of each D candidate are constrained to come from a common vertex. Additionally, for the $D^0 \to K^-\pi^+\pi^0$ channel, the D^0 mass constraint is included in the fit, and for the $D^- \to K^0_S\pi^-$ channel, a K^0_S mass constraint is imposed. Reconstructed D candidates with a χ^2 fit probability greater than 0.1% are retained. Each $D\bar{D}$ pair is refit to a common vertex with the constraint that the pair originates from the e^+e^- interaction region. Only candidates with a χ^2 fit probability greater than 0.1% are retained. Background π^0 candidates from random combinations of photons and other background channels are suppressed by requiring no more than one π^0 candidate other than those attributed to the D^0 and D^* decays. Similarly, we require in the event no more than one extra photon candidate, having a minimum energy of 100 MeV, apart from any photon attributed to D^* or π^0 decays.

For D decay modes without a π^0 daughter, the D-candidate momentum is determined from the summed three-momenta of the decay particles, and its energy is computed using the nominal D mass value [9]. For the $D^0 \to K^-\pi^+\pi^0$ channel, the four-momentum from the mass-constrained fit is used. Similarly, the D^* momentum is determined from the summed three-momenta of the decay particles and its energy is computed using the nominal D^* mass.

The ISR photon is preferentially emitted at small angles with respect to the beam axis, and escapes detection in the majority of ISR events. Consequently, the ISR photon is treated as a missing particle. We define the squared mass ($M^2_{\rm rec}$) recoiling against the $D\bar{D}$, $D^*\bar{D}$, and $D^*\bar{D}^*$ systems using the four-momenta of the beam particles ($p_{e^\pm}$) and of the reconstructed $D(p_D)$ and $D^*(p_{D^*})$

$$M^2_{\rm rec} \equiv (p_{e^-} + p_{e^+} - p_{D^{(*)}} - p_{\bar{D}^{(*)}})^2. \quad (1)$$

This quantity should peak near zero for both ISR events and for exclusive production of $e^+e^- \to D^*\bar{D}$ or $e^+e^- \to D^*\bar{D}^*$. In exclusive production the $D^*\bar{D}$ and $D^*\bar{D}^*$ mass distributions peak at the kinematic limit. Therefore, we select ISR candidates by requiring $D\bar{D}$, $D^*\bar{D}$, and $D^*\bar{D}^*$ invariant masses below 6 GeV/c^2 and $|M^2_{\rm rec}| < 1$ GeV$^2/c^4$.

We select D and D^* candidates based on the candidate D mass and the mass difference $\Delta m = M_{D^*} - M_D$. The D and D^* parameters are obtained by fitting the relevant mass spectra (see Fig. 1 for some Δm distributions) using a polynomial for the background and a single Gaussian for the signal. Events are selected within $\pm 2.5\sigma$ from the fitted central values, where σ is the Gaussian width. For $D^{*+} \to D^0\pi^+$, the selection criterion has been extended to $\pm 6\sigma$ due to the presence of non-Gaussian tails.

Because of our tolerance of an extra π^0 and/or γ, an ambiguity can occur for channels involving a D^{*0}, which is handled as follows. Each combination is considered as a possible candidate for channels 8–12 and $D^0\bar{D}^0$. Monte Carlo simulations weighted by the $D\bar{D}$, $D^*\bar{D}$, and $D^*\bar{D}^*$ measured cross sections [15–17], and branching fractions are used to optimize the selection criteria and estimate the feedthrough of one channel to the other. A candidate is rejected if (a) it satisfies all the selection criteria for an ambiguous channel and (b) this rejection

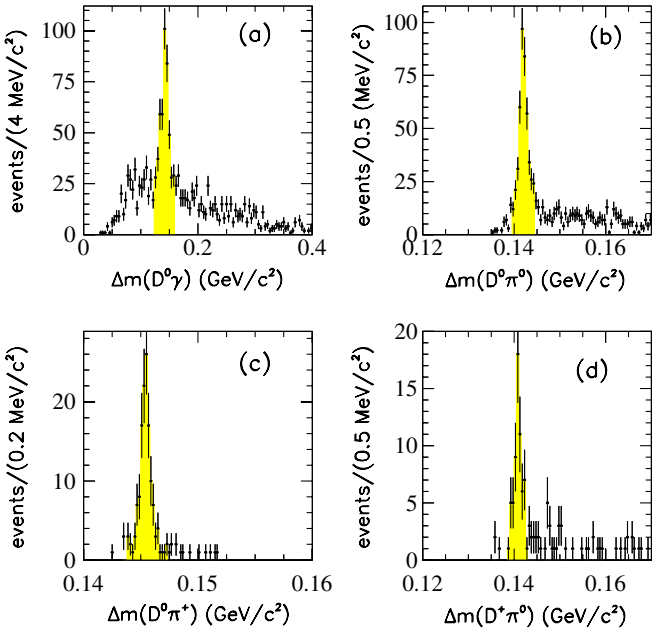

FIG. 1 (color online). Δm distributions for $D^*\bar{D}$ candidates after applying the $|M^2_{\rm rec}| < 1$ GeV$^2/c^4$ and $m(D^*\bar{D}) < 6$ GeV$/c^2$ selections, for (a) $D^{*0} \to D^0\gamma$, (b) $D^{*0} \to D^0\pi^0$, (c) $D^{*+} \to D^0\pi^+$ with $D^0 \to K^-\pi^+$, and (d) $D^{*+} \to D^+\pi^0$ with $D^+ \to K^-\pi^+\pi^+$. The shaded regions indicate the ranges used to select the D^* candidates.

does not produce any significant loss in the channel under study and therefore can be classified as background. The list of channels rejected in case of ambiguities are indicated in the ''Veto'' column in Table II. The table also lists the fraction of events removed by these cuts in the $|M^2_{\rm rec}| < 1$ GeV$^2/c^4$ region.

In the case of multiple D^{*0} candidates, such as $D^{*0}\bar{D}^{*0}$ with both $D^{*0} \to D^0\gamma$, the candidate with $m(D^0\gamma)$ closest to the nominal D^{*0} mass is accepted. The charged $D^*\bar{D}$ and $D^*\bar{D}^*$ modes, also listed in Table II, do not require such a procedure because backgrounds are negligible.

IV. STUDY OF THE $D^*\bar{D}$ FINAL STATE

Figure 2 shows the $D^*\bar{D}M^2_{\rm rec}$ distributions after all the cuts for (a) $D^{*0}\bar{D}^0$, $D^{*0} \to D^0\gamma$, (b) $D^{*0}\bar{D}^0$, $D^{*0} \to D^0\pi^0$, and (c) $D^{*+}D^-$. Clear peaks centered at zero with little background are observed, providing evidence of an ISR process.

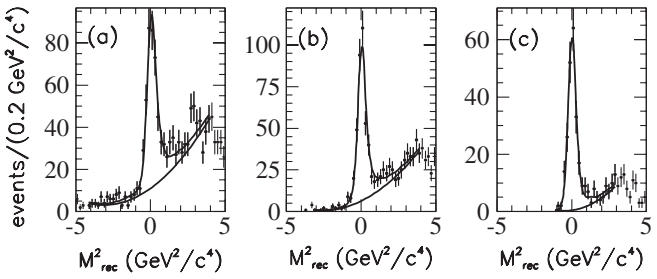

FIG. 2. Distribution of $M^2_{\rm rec}$, the mass recoiling against the $D^*\bar{D}$ system, for (a) $D^{*0} \to D^0\gamma$, (b) $D^{*0} \to D^0\pi^0$, and (c) $D^{*+}D^-$ candidates. The curves are the results from the fits described in the text.

The number of background events in the $|M^2_{\rm rec}| < 1$ GeV$^2/c^4$ is estimated by fitting the $M^2_{\rm rec}$ distribution for each channel. The fits are performed using a 2^{nd} order polynomial for the background and a signal $M^2_{\rm rec}$ lineshape obtained from Monte Carlo simulations corresponding to the relative composition of the data. The event yields are obtained by subtracting the fitted backgrounds and integrating the resulting $M^2_{\rm rec}$ distributions in the $|M^2_{\rm rec}| < 1$ GeV$^2/c^4$ region. The resulting yields and fitted purities, defined as $P = N_{\rm signal}/(N_{\rm signal} + N_{\rm background})$, for each channel are summarized in Table III.

The purity of each reconstructed D^* channel is also demonstrated in Fig. 1, where the Δm distribution is shown for $D^*\bar{D}$ candidates with $|M^2_{\rm rec}| < 1$ GeV$^2/c^4$ and $D^*\bar{D}$ masses below 6 GeV$/c^2$. The final selection of the ISR candidates is performed applying the Δm selection criteria described above.

The $D^{*0}\bar{D}^0$ mass spectrum is shown in Fig. 3(a), and the $D^{*+}D^-$ mass spectrum is shown in Fig. 3(b). Both spectra show an enhancement near threshold due to the presence of the $\psi(4040)$ resonance.

The background shape for $D^{*0}\bar{D}^0$ candidates is explored using the $M^2_{\rm rec}$ sideband region, $1.5 < M^2_{\rm rec} < 3.5$ GeV$^2/c^4$. The $D^{*0}\bar{D}^0$ mass spectrum for these events, normalized to the background estimated from the fit to the $M^2_{\rm rec}$ distribution, is presented as the shaded histogram in Fig. 3(a). This background has been fitted with a threshold function

$$B(m) = (m - m_{th})^{\alpha+\beta m} e^{-\gamma m - \delta m^2 - \epsilon m^3}, \qquad (2)$$

where m_{th} is the threshold $D^{*0}\bar{D}^0$ mass. The $D^{*+}D^-$ final state is consistent with having zero background.

V. MASS RESOLUTION, EFFICIENCY, AND $D^*\bar{D}$ CROSS SECTION

In order to measure efficiencies and $D^*\bar{D}$ mass resolutions, ISR events are simulated at five different values of the $D^*\bar{D}$ invariant masses between 4.25 and 6.25 GeV$/c^2$. These events are simulated using the GEANT4 detector simulation package [20] and are processed through the same reconstruction and analysis chain as real events. The mass resolution is determined from the difference between generated and reconstructed $D^*\bar{D}$ masses. The $D^*\bar{D}$ mass resolutions are similar for all channels and increase with $D^*\bar{D}$ mass from 5 to 10 MeV$/c^2$.

The mass-dependent reconstruction efficiency for channel i, $\epsilon_i(m_{D^*\bar{D}})$ is parameterized by a second-order polynomial, and is multiplied by the decay branching fraction $\mathcal{B}_i$ [9] to define

$$\epsilon_i^{\mathcal{B}}(m_{D^*\bar{D}}) = \epsilon_i(m_{D^*\bar{D}}) \times \mathcal{B}_i. \qquad (3)$$

These values are weighted by $N_i(m_{D^*\bar{D}})$, the number of

TABLE III. Number of ISR candidates and purities for the different channels calculated in the range $|M^2_{\rm rec}| < 1$ GeV$^2/c^4$. The last column gives the value of the average efficiency $\epsilon^{\mathcal{B}}$ at a mass of 4.5 GeV$/c^2$.

Channel	Signal + Background	Purity(%)	$\epsilon^{\mathcal{B}} \times 10^{-5}$
$D^0\bar{D}^0$	654	74.3 ± 1.7	
D^+D^-	199	88.4 ± 2.3	
Total $D\bar{D}$	853	77.6 ± 1.4	25
$D^{*0}\bar{D}^0$, $D^{*0} \to D^0\gamma$	460	75.4 ± 2.0	
$D^{*0}\bar{D}^0$ $D^{*0} \to D^0\pi^0$	422	84.4 ± 1.8	
Total $D^{*0}\bar{D}^0$	882	79.7 ± 1.4	4
$D^{*+}D^-$	228	100^{+0}_{-3}	5
Total $D^*\bar{D}$	1110	83.6 ± 1.1	
$D^{*0}\bar{D}^{*0}$	293	69.3 ± 3.7	
$D^{*+}D^{*-}$	33	100^{+0}_{-3}	
Total $D^*\bar{D}^*$	326	72.1 ± 2.5	1

$D^*\bar{D}$ candidates in channel i, to compute the average efficiency as a function of $m_{D^*\bar{D}}$,

$$\epsilon^{\mathcal{B}}(m_{D^*\bar{D}}) = \frac{\sum_{i=1}^{n} N_i(m_{D^*\bar{D}})}{\sum_{i=1}^{n} \frac{N_i(m_{D^*\bar{D}})}{\epsilon_i^{\mathcal{B}}(m_{D^*\bar{D}})}}, \tag{4}$$

where n is the number of decay modes. In this case, we have eight $D^{*0}\bar{D}^0$ channels (1–4 with $D^{*0} \to D^0\gamma$ and $D^{*0} \to D^0\pi^0$) and two $D^{*+}D^-$ channels (13, 14). Representative values of $\epsilon^{\mathcal{B}}$, computed at a mass of 4.5 GeV$/c^2$, are displayed in Table III. The sample sizes

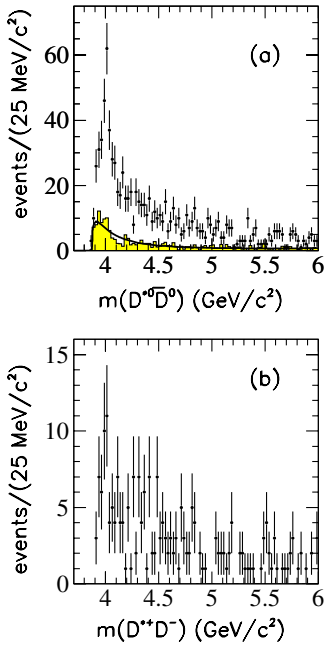

FIG. 3 (color online). (a) $D^{*0}\bar{D}^0$ and (b) $D^{*+}D^-$ mass spectra. The shaded histogram in (a) is obtained from the $M^2_{\rm rec}$ sideband region $1.5 < M^2_{\rm rec} < 3.5$ GeV$^2/c^4$ normalized to the background estimated from the fit to the $M^2_{\rm rec}$ distribution. The curve is the result from the fit described in the text.

for the Cabibbo-suppressed decay modes (15, 16, and 17 in Table II) are very small (32 events total) and comprise 14% of the $D^{*+}D^-$ sample. The efficiency for these decay channels has not been directly computed; instead, these modes are treated as having the mean efficiency of the Cabibbo-allowed channels 13 and 14. The ten $D^*\bar{D}$ channels, after correcting for efficiency and branching fractions, have yields that are consistent within the statistical errors.

The $D^*\bar{D}$ cross section is computed using

$$\sigma_{e^+e^-\to D^*\bar{D}}(m_{D^*\bar{D}}) = \frac{dN/dm_{D^*\bar{D}}}{\epsilon^{\mathcal{B}}(m_{D^*\bar{D}}) d\mathcal{L}/dm_{D^*\bar{D}}}, \tag{5}$$

where $dN/dm_{D^*\bar{D}}$ is the background-subtracted yield. The differential luminosity is computed as [21]

$$\frac{d\mathcal{L}}{dm_{D^*\bar{D}}} = \mathcal{L}\frac{2m_{D^*\bar{D}}}{s}\frac{\alpha}{\pi x}(\ln(s/m_e^2) - 1)(2 - 2x + x^2), \tag{6}$$

where s is the square of the e^+e^- center-of-mass energy, α is the fine-structure constant, $x = 1 - m^2_{D^*\bar{D}}/s$, m_e is the electron mass, and $\mathcal{L}$ is the integrated luminosity of 384 fb^{-1}. The cross sections for $D^{*0}\bar{D}^0$, $D^{*+}D^-$, and combined $D^{*0}\bar{D}^0$ and $D^{*+}D^-$ are shown in Fig. 4. A clear $\psi(4040)$ resonance is observed.

The systematic uncertainties on the cross sections, 10.9% for $D^{*0}\bar{D}^0$ and 9.3% for $D^{*+}D^-$, include uncertainties for particle identification, tracking, photon and π^0 reconstruction efficiencies, background estimates, branching fractions, and a potential inaccuracy in the simulation of extraneous tracks, photon, and π^0 candidates. The uncertainty due to the ISR selection has been estimated by narrowing the $M^2_{\rm rec}$ allowed range to 0.7 GeV$^2/c^4$. All contributions are added in quadrature. Systematic uncertainties are summarized in Table IV.

The $D^{*0}\bar{D}^0$ and $D^{*+}D^-$ cross sections have similar features and consistent yields. Integrating the cross sec-

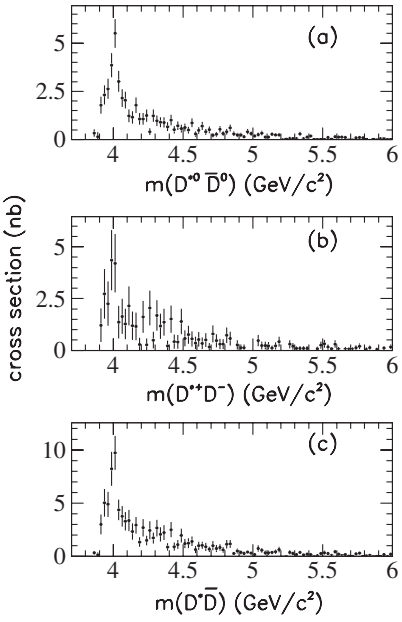

FIG. 4. Cross section for $e^+e^- \to$ (a) $D^{*0}\bar{D}^0$, (b) $D^{*+}D^-$, and (c) $D^*\bar{D}$ combined. The error bars correspond to statistical errors only.

TABLE IV. Systematic errors, given as fractional errors expressed in %, in the evaluation of the $D^*\bar{D}$ cross section.

Effect	$D^{*0}\bar{D}^0$	$D^{*+}D^-$
Background subtraction	2.6	3.0
Branching fractions	7.4	4.6
$M^2_{\rm rec}$ cut	2.2	0.0
Particle identification	1.8	2.1
Tracking efficiency	2.2	3.3
Extraneous tracks	5.7	5.7
π^0 and γ reconstruction efficiency	3.4	3.0
Extraneous π^0 and γ	0.5	0.8
Total	10.9	9.3

tions from threshold to 6 GeV$/c^2$, we obtain

$$\frac{\sigma(D^{*+}D^-)}{\sigma(D^{*0}\bar{D}^0)} = 0.95 \pm 0.09_{\rm stat} \pm 0.10_{\rm syst}, \qquad (7)$$

consistent with unity. In this calculation systematic errors related to the $M^2_{\rm rec}$ selection criteria and tracking efficiency have been ignored because they largely cancel in the ratio.

VI. STUDY OF THE $D^*\bar{D}^*$ SYSTEM

A similar analysis is carried out for $D^*\bar{D}^*$ channels. Figure 5 shows the Δm distributions for $D^*\bar{D}^*$ candidates with $|M^2_{\rm rec}| < 1$ GeV$^2/c^4$ and $D^*\bar{D}^*$ masses below 6 GeV$/c^2$. The peak at threshold in Fig. 5(a) is due to background from $D^{*0} \to D^0\pi^0$ where one γ from the low momentum π^0 is lost.

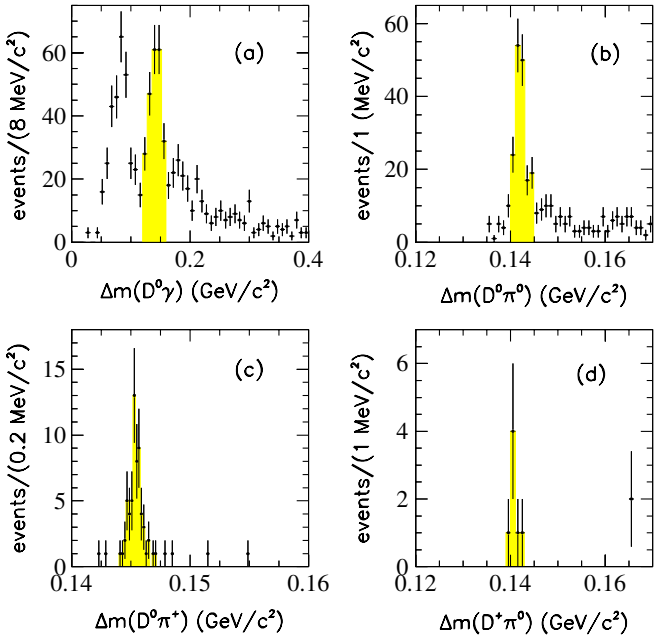

FIG. 5 (color online). Δm distributions for $D^*\bar{D}^*$ candidates after applying the $|M^2_{\rm rec}| < 1$ GeV$^2/c^4$ and $m(D^*\bar{D}^*) < 6$ GeV$/c^2$ selections, for (a) $D^{*0} \to D^0\gamma$, (b) $D^{*0} \to D^0\pi^0$, (c) $D^{*+} \to D^0\pi^+$ with $D^0 \to K^-\pi^+$, and (d) $D^{*+} \to D^+\pi^0$ with $D^+ \to K^-\pi^+\pi^+$. The shaded regions indicate the ranges used to select the D^* signals.

We select the two D^* candidates and reject candidates reconstructed in any of the modes listed in the Veto column in Table II. Figure 6 shows the $D^{*0}\bar{D}^{*0}$ $M^2_{\rm rec}$ distributions for channels 10–12.

The total $D^{*0}\bar{D}^{*0}$ and $D^{*+}D^{*-}$ $M^2_{\rm rec}$ distributions are shown in Fig. 7. The number of background events for the $D^{*0}\bar{D}^{*0}$ channel is estimated by fitting the $M^2_{\rm rec}$ distribution. The fit is performed using a 2^{nd}-order polynomial for the background and a signal $M^2_{\rm rec}$ lineshape obtained from Monte Carlo simulations that reflect the composition of the data. The number of ISR candidates and purities are also summarized in Table III. The $D^{*+}D^{*-}$ final state has a background consistent with zero.

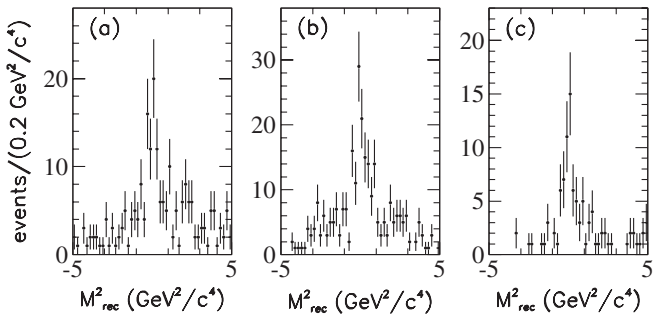

FIG. 6. $M^2_{\rm rec}$ distributions for $D^{*0}\bar{D}^{*0}$ for (a) $D^{*0} \to D^0\gamma$, $\bar{D}^{*0} \to \bar{D}^0\gamma$, (b) $D^{*0} \to D^0\pi^0$, $\bar{D}^{*0} \to \bar{D}^0\gamma$, and (c) $D^{*0} \to D^0\pi^0$, $\bar{D}^{*0} \to \bar{D}^0\pi^0$.

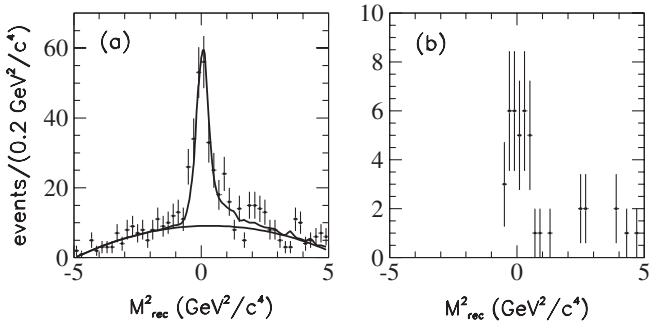

FIG. 7. $M^2_{\rm rec}$ distributions for (a) $D^{*0}\bar{D}^{*0}$ and (b) $D^{*+}D^{*-}$. The curve in (a) is the result from the fit described in the text.

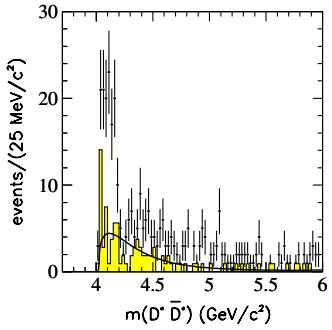

FIG. 8 (color online). $D^*\bar{D}^*$ mass spectrum. The shaded histogram is obtained from the $M^2_{\rm rec}$ sidebands $-2.5 < M^2_{\rm rec} < -1.5$ and $1.5 < M^2_{\rm rec} < 2.5$ GeV$^2/c^4$. The curve is the result from the fit described in the text.

Because of the small $D^{*+}D^{*-}$ sample size, the charged and neutral mass spectra are summed in Fig. 8. The $D^*\bar{D}^*$ mass spectrum shows unresolved peaks at $\psi(4040)$ and $\psi(4160)$ and an enhancement at the position of the $\psi(4400)$ [9].

The background is explored using events in the $M^2_{\rm rec}$ sideband regions $-2.5 < M^2_{\rm rec} < -1.5$ GeV$^2/c^4$ and $1.5 < M^2_{\rm rec} < 2.5$ GeV$^2/c^4$, and fitted using Eq. (2). The $D^*\bar{D}^*$ mass spectrum for these events, normalized from the fit to the $M^2_{\rm rec}$ distribution, is shown as the shaded histogram in Fig. 8.

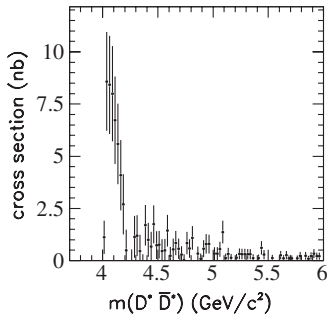

FIG. 9. Cross section $e^+e^- \to D^*\bar{D}^*$ for combined $D^{*0}\bar{D}^{*0}$ and $D^{*+}D^{*-}$. Error bars indicate the statistical errors only.

TABLE V. Systematic errors, given as fractional errors expressed in %, in the evaluation of the $D^*\bar{D}^*$ cross section.

Effect	Fraction (%)
Background subtraction	2.1
Branching fractions	9.3
$M^2_{\rm rec}$ cut	1.3
Particle identification	2.8
Tracking efficiency	2.6
Extraneous tracks	5.7
π^0 and γ reconstruction efficiency	4.1
Total	12.4

The $D^*\bar{D}^*$ cross section is calculated using the same method used to compute the $D^*\bar{D}$ cross section. The result, summed over the neutral and charged modes, is shown in Fig. 9. All systematic uncertaintiesthat have been taken into account for the $D^*\bar{D}^*$ mode are listed in Table V; the overall uncertainty on the cross section is 12.4%.

The $D^*\bar{D}^*$ cross section distribution exhibits a threshold enhancement due to the superposition of the $\psi(4040)$ and $\psi(4160)$ resonances.

VII. THE $D\bar{D}$ MASS SPECTRUM

In the selection of the $D^0\bar{D}^0$ sample we also apply the method of resolving ambiguous events having an addi-

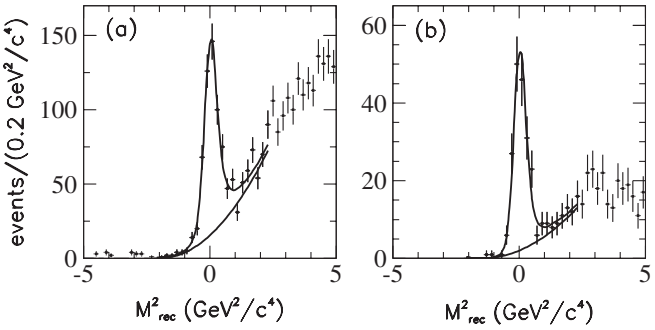

FIG. 10. $M^2_{\rm rec}$ distribution for (a) $D^0\bar{D}^0$ and (b) D^+D^-. The curves are the results from the fits described in the text.

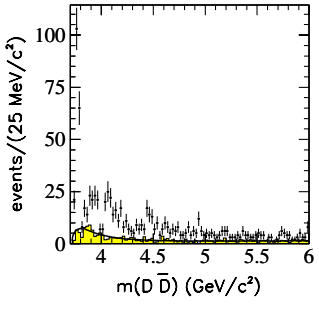

FIG. 11 (color online). $D\bar{D}$ mass distribution. The shaded histogram is obtained from the $M^2_{\rm rec}$ sideband. The curve is the result from the fit described in the text.

tional π^0 and/or γ. Here, we Veto all events that are ambiguous with channels 8–12, obtaining a rejection of 7.6% background events in the $|M^2_{\rm rec}| < 1\ {\rm GeV}^2/c^4$ region. No such procedure is applied to the D^+D^- sample. The $D\bar{D}$ analysis is otherwise identical to that reported in Ref. [15]. The resulting $M^2_{\rm rec}$ distributions for $D^0\bar{D}^0$ and D^+D^- channels are shown in Fig. 10. The curves are the results from the fits performed using a 2^{nd} order polynomial for the background and a $M^2_{\rm rec}$ lineshape obtained from Monte Carlo simulations that reflect the channel composition of the data. Again, the resulting event yields and purities are summarized in Table III.

The combined $D\bar{D}$ mass spectrum is shown in Fig. 11. The background is explored using events in the $M^2_{\rm rec}$ sideband regions $1.5 < M^2_{\rm rec} < 3.5\ {\rm GeV}^2/c^4$ and fitted using Eq. (2). This background, normalized from the fit to the $M^2_{\rm rec}$ distributions, is shown as the shaded histogram in Fig. 11.

The features in the $D\bar{D}$ mass spectrum and the resulting $D\bar{D}$ cross section have been extensively discussed in our previous publication [15].

VIII. FIT TO THE MASS SPECTRA

Unbinned maximum likelihood fits to the $D^0\bar{D}^0$, D^+D^-, $D^{*0}\bar{D}^0$, $D^{*+}D^-$, $D^{*0}\bar{D}^{*0}$, and $D^{*+}D^{*-}$ mass spectra are performed. We write the likelihood functions as

$$L = f\epsilon^{\mathcal{B}}(m)|P(m) + c_1W_1(m)e^{i\phi_1} + c_2\sqrt{G(m)}e^{i\phi_2} + \ldots + c_nW_n(m)e^{i\phi_n}|^2 + B(m)(1-f), \quad (8)$$

where m is the $D^{(*)}\bar{D}^{(*)}$ mass, c_i and ϕ_i are free parameters, $W_i(m)$ are P-wave relativistic Breit-Wigner distributions [9], $P(m)$ represents the nonresonant contribution, $B(m)$ describes the background, $\epsilon^{\mathcal{B}}(m)$ is the average efficiency, and f is the signal fraction fixed to the values obtained fitting the $M^2_{\rm rec}$ distributions.

The parameters of the $\psi(4040)$, $\psi(4160)$, and $\psi(4415)$ are fixed to the values reported in the Review of Particle Physics [9]. The parameters of the $\psi(3770)$ are fixed to the values obtained in our previous analysis of the $D\bar{D}$ system [15]. The $D\bar{D}$ data require that we include the 3.9 ${\rm GeV}/c^2$ structure, as suggested in Ref. [22], which we parametrize empirically as the square root of a Gaussian times a phase factor $\sqrt{G(m)}e^{i\phi_2}$. The parameters of the Gaussian are fixed to the values obtained in our previous analysis of the $D\bar{D}$ system: $m_{G(3900)} = 3943 \pm 17\ {\rm MeV}/c^2$, $\sigma_{G(3900)} = 52 \pm 8\ {\rm MeV}/c^2$ [15]. The shape of the nonresonant contribution $P(m)$ is unknown; we therefore parametrize it in a simple way as

$$P(m) = C(m)(a + bm), \quad (9)$$

where $C(m)$ is the phase space function for $D^{(*)}\bar{D}^{(*)}$, and a and b are free parameters. Resolution effects have been ignored since the widths of the resonances are much larger than the experimental resolution.

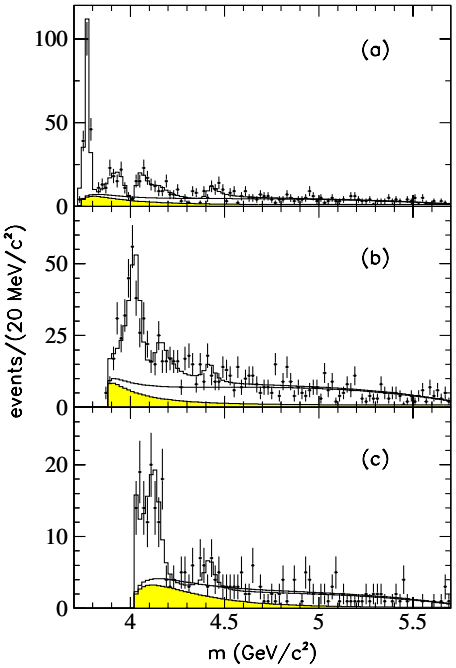

FIG. 12 (color online). Fits to the (a) $D\bar{D}$, (b) $D^*\bar{D}$, and (c) $D^*\bar{D}^*$ mass spectra. Data are represented with error bars, the curves represent the fitted functions. The shaded histogram corresponds to the smoothed incoherent background ($B(m)$) estimated from sidebands. The second smooth solid line represents the nonresonant contribution ($|P(m)|^2$).

Interference between the resonances and the nonresonant contribution $P(m)$ is required to obtain a satisfactory description of the data. The size of the nonresonant production is determined by the fit.

The six $D^0\bar{D}^0$, D^+D^-, $D^{*0}\bar{D}^0$, $D^{*+}D^-$, $D^{*0}\bar{D}^{*0}$, and $D^{*+}D^{*-}$ likelihood functions are computed with different thresholds, efficiencies, purities, backgrounds, and numbers of contributing resonances appropriate for each channel. The fits, summed over the charged and neutral final states, are shown in Fig. 12; they provide a good description of all the data. In the figure, the shaded areas indicate the background estimated by fitting the $M^2_{\rm rec}$ sidebands. The second smooth solid line represents the nonresonant contribution where we plot $|P(m)|^2$, therefore ignoring the interference effects.

The fraction for each resonant contribution i is defined by the following expression:

$$f_i = \frac{|c_i|^2 \int |W_i(m)|^2 dm}{\sum_{j,k} c_j c_k^* \int W_j(m) W_k^*(m) dm}. \quad (10)$$

The fractions f_i do not necessarily add up to 1 because of interference between amplitudes. The error for each fraction has been evaluated by propagating the full covariance matrix obtained by the fit. The resulting fit fractions and phases are given in Table VI.

TABLE VI. $D\bar{D}$, $D^*\bar{D}$, and $D^*\bar{D}^*$ fit fractions (in %) and phases. Errors are statistical only.

Res.	$D\bar{D}$ fraction	$D\bar{D}$ phase	$D^*\bar{D}$ fraction	$D^*\bar{D}$ phase	$D^*\bar{D}^*$ fraction	$D^*\bar{D}^*$ phase
$\|P\|^2$	38.5 ± 7.1	0.	49.9 ± 5.6	0.	56.8 ± 9.2	0.
$\psi(3770)$	31.3 ± 3.3	1.58 ± 0.46				
$G(3900)$	23.9 ± 5.8	5.46 ± 0.64				
$\psi(4040)$	31.2 ± 5.3	1.39 ± 0.55	34.5 ± 6.0	1.74 ± 0.33	5.7 ± 4.4	3.37 ± 0.48
$\psi(4160)$	3.1 ± 3.3	2.75 ± 0.58	12.2 ± 3.8	2.26 ± 0.16	30.6 ± 7.3	5.94 ± 0.33
$\psi(4400)$	2.0 ± 1.2	3.38 ± 0.37	0.6 ± 0.7	4.37 ± 0.47	3.6 ± 2.4	5.03 ± 0.45
Sum	130 ± 12		97 ± 8		97 ± 13	

TABLE VII. Integrated rates (in nb · MeV) for $e^+e^- \to \psi(4040)$, $e^+e^- \to \psi(4160)$, and $e^+e^- \to \psi(4400)$ in the $D\bar{D}$, $D^*\bar{D}$, and $D^*\bar{D}^*$ decay modes. The first error is statistical, the second systematic.

Decay mode	$\psi(4040)$	$\psi(4160)$	$\psi(4400)$
$D\bar{D}$	$11.0 \pm 1.8 \pm 5.6$	$1.0 \pm 1.3 \pm 1.0$	$0.5 \pm 0.3 \pm 0.1$
$D^*\bar{D}$	$46.6 \pm 7.0 \pm 4.9$	$13.8 \pm 4.4 \pm 1.5$	$0.6 \pm 0.8 \pm 0.1$
$D^*\bar{D}^*$	$8.3 \pm 6.4 \pm 1.0$	$40.6 \pm 9.7 \pm 5.0$	$3.6 \pm 2.4 \pm 0.4$

IX. FIT FRACTIONS AND INTEGRATED RATES

The fit gives corrected yields for each charmonium resonance. Since the fits have been performed independently for the neutral and charged modes, the weighted means of the fit fractions are used. These can be used to compute the integrated rates for each resonance in the $D\bar{D}$, $D^*\bar{D}$, and $D^*\bar{D}^*$ decay modes, which are reported in Table VII.

The systematic errors take into account uncertainties on resonance parameters, Breit-Wigner lineshapes, branching fractions, and background estimates. The nonresonant contribution has been parametrized in an alternative way, $P(m) = C(m)e^{a+bm}$. Each resonance parameter has been varied according to its uncertainty, and the meson radius used in the Blatt-Weisskopf damping factor [23], which is present in each relativistic Breit-Wigner term, has been varied between 0 and 2.5 GeV^{-1}. The amounts of backgrounds in the different final states have been varied according to their errors. The 3.9 GeV/c^2 structure in the $D\bar{D}$ mass spectrum has been alternatively described by a P-wave relativistic Breit Wigner with free parameters. This effect dominates the systematic uncertainty on the $\psi(4040)$ rate in the $D\bar{D}$ mass spectrum. The deviations from the central value are added in quadrature. Systematic effects also include the uncertainty on the total cross sections.

The corrected yields can also be used to compute the branching fraction ratios. The results are shown in Table VIII together with predictions of models: significant discrepancies are observed, especially with the $^3P_0$ model [5].

X. LIMITS ON THE DECAYS $Y(4260) \to D^*\bar{D}$ AND $Y(4260) \to D^*\bar{D}^*$

The $D^*\bar{D}$ and $D^*\bar{D}^*$ mass spectra have been refit with an additional $Y(4260)$ resonance, which is allowed to interfere with all the other terms.

The fit gives $Y(4260)$ fractions of $(2.2 \pm 2.9_{\mathrm{stat}} \pm 2.5_{\mathrm{syst}})\%$ and $(4.0 \pm 2.0_{\mathrm{stat}} \pm 4.2_{\mathrm{syst}})\%$ corresponding to $18 \pm 24_{\mathrm{stat}} \pm 21_{\mathrm{syst}}$ and $9 \pm 5_{\mathrm{stat}} \pm 10_{\mathrm{syst}}$ events for $Y(4260) \to D^*\bar{D}$ and $Y(4260) \to D^*\bar{D}^*$, respectively. Systematic errors due to uncertainties on masses and widths of the $\psi(4040)$, $\psi(4160)$, $\psi(4415)$, and $Y(4260)$ resonances are evaluated by varying the masses and widths

TABLE VIII. Ratios of branching fractions for the three ψ resonances. The first error is statistical, the second systematic. Theoretical expectations are from the $^3P_0$ model [5], C^3 model [6], and $\rho K \rho$ model [14].

Ratio	Measurement	$^3P_0$	C^3 and $\rho K \rho$
1) $\mathcal{B}(\psi(4040) \to D\bar{D})/\mathcal{B}(\psi(4040) \to D^*\bar{D})$	$0.24 \pm 0.05 \pm 0.12$	0.003	0.14 [14]
2) $\mathcal{B}(\psi(4040) \to D^*\bar{D}^*)/\mathcal{B}(\psi(4040) \to D^*\bar{D})$	$0.18 \pm 0.14 \pm 0.03$	1.0	0.29 [14]
3) $\mathcal{B}(\psi(4160) \to D\bar{D})/\mathcal{B}(\psi(4160) \to D^*\bar{D}^*)$	$0.02 \pm 0.03 \pm 0.02$	0.46	0.08 [6]
4) $\mathcal{B}(\psi(4160) \to D^*\bar{D})/\mathcal{B}(\psi(4160) \to D^*\bar{D}^*)$	$0.34 \pm 0.14 \pm 0.05$	0.011	0.16 [6]
5) $\mathcal{B}(\psi(4400) \to D\bar{D})/\mathcal{B}(\psi(4400) \to D^*\bar{D}^*)$	$0.14 \pm 0.12 \pm 0.03$	0.025	
6) $\mathcal{B}(\psi(4400) \to D^*\bar{D})/\mathcal{B}(\psi(4400) \to D^*\bar{D}^*)$	$0.17 \pm 0.25 \pm 0.03$	0.14	

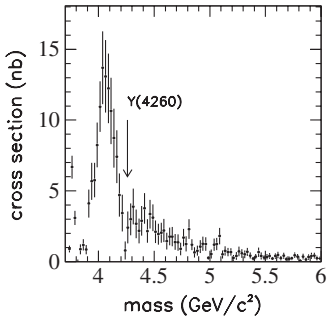

FIG. 13. Sum of $e^+e^- \to D\bar{D}$, $e^+e^- \to D^*\bar{D}$, and $e^+e^- \to D^*\bar{D}^*$ cross sections. The arrow indicates the position of the $Y(4260)$.

by their uncertainty in the fit. The amount of background in each final state is varied within its statistical error, and the meson radii in Breit-Wigner terms are varied between 0 and 2.5 GeV^{-1}. Deviations from the central value are added in quadrature.

These $Y(4260)$ yields in the $D^*\bar{D}$ and $D^*\bar{D}^*$ channels are used to compute the cross section times branching fraction, which can then be compared to our measurement from the $J/\psi\pi^+\pi^-$ channel [2]. We obtain

$$\frac{\mathcal{B}(Y(4260) \to D^*\bar{D})}{\mathcal{B}(Y(4260) \to J/\psi\pi^+\pi^-)} < 34, \tag{11}$$

and

$$\frac{\mathcal{B}(Y(4260) \to D^*\bar{D}^*)}{\mathcal{B}(Y(4260) \to J/\psi\pi^+\pi^-)} < 40 \tag{12}$$

at the 90% confidence level.

Using the $D\bar{D}$ cross section measured in the earlier *BABAR* work [15], we obtain the sum of the $e^+e^- \to D\bar{D}$, $e^+e^- \to D^*\bar{D}$, and $e^+e^- \to D^*\bar{D}^*$ cross sections shown in Fig. 13: the arrow indicates the position of the $Y(4260)$, which falls in a local minimum, in agreement with the cross section measured for hadron production in e^+e^- annihilation [9].

XI. CONCLUSIONS

We have studied the exclusive ISR production of the $D\bar{D}$, $D^*\bar{D}$, and $D^*\bar{D}^*$ systems. The mass spectra show production of the $J^{PC} = 1^{--}$ states $\psi(3770)$, $\psi(4040)$, $\psi(4160)$, and $\psi(4415)$. Fits to the mass spectra provide amplitudes and relative phases for the charmonium states, from which first measurements of branching fraction ratios are obtained. Finally, upper limits on $Y(4260) \to D^*\bar{D}$ and $Y(4260) \to D^*\bar{D}^*$ decays are computed.

If the $Y(4260)$ is a 1^{--} charmonium state, it should decay predominantly to $D\bar{D}$, $D^*\bar{D}$, and $D^*\bar{D}^*$ [5,6]. Within the present limited data sample size, no evidence is found for $Y(4260)$ decays to $D\bar{D}$, $D^*\bar{D}$, or $D^*\bar{D}^*$. Other explanations for the $Y(4260)$ have been proposed, such as a hybrid, baryonium, molecule or tetraquark state. In the case of a hybrid state, the decay rates to $D\bar{D}$, $D^*\bar{D}$, and $D^*\bar{D}^*$ are expected to be small [10,24].

ACKNOWLEDGMENTS

We are grateful for the extraordinary contributions of our PEP-II colleagues in achieving the excellent luminosity and machine conditions that have made this work possible. The success of this project also relies critically on the expertise and dedication of the computing organizations that support *BABAR*. The collaborating institutions wish to thank SLAC for its support and the kind hospitality extended to them. This work is supported by the U.S. Department of Energy and National Science Foundation, the Natural Sciences and Engineering Research Council (Canada), the Commissariat à l'Energie Atomique and Institut National de Physique Nucléaire et de Physique des Particules (France), the Bundesministerium für Bildung und Forschung and Deutsche Forschungsgemeinschaft (Germany), the Istituto Nazionale di Fisica Nucleare (Italy), the Foundation for Fundamental Research on Matter (The Netherlands), the Research Council of Norway, the Ministry of Education and Science of the Russian Federation, Ministerio de Educación y Ciencia (Spain), and the Science and Technology Facilities Council (United Kingdom). Individuals have received support from the Marie Curie IEF program (European Union) and the A. P. Sloan Foundation.

[1] S.-K. Choi *et al.* (Belle Collaboration), Phys. Rev. Lett. **91**, 262001 (2003).
[2] B. Aubert *et al.* (*BABAR* Collaboration), Phys. Rev. Lett. **95**, 142001 (2005).
[3] B. Aubert *et al.* (*BABAR* Collaboration), Phys. Rev. Lett. **98**, 212001 (2007).
[4] X. L. Wang *et al.* (Belle Collaboration), Phys. Rev. Lett. **99**, 142002 (2007).
[5] T. Barnes, S. Godfrey, and E. S. Swanson, Phys. Rev. D **72**, 054026 (2005).
[6] E. J. Eichten, K. Lane, and C. Quigg, Phys. Rev. D **73**, 014014 (2006).
[7] Charge conjugate states are implied throughout this work.
[8] X. H. Mo *et al.*, Phys. Lett. B **640**, 182 (2006).

[9] C. Amsler *et al.*, Phys. Lett. B **667**, 1 (2008).
[10] S. L. Zhu, Phys. Lett. B **625**, 212 (2005); E. Kou and O. Pene, Phys. Lett. B **631**, 164 (2005); F. E. Close and P. R. Page, Phys. Lett. B **628**, 215 (2005).
[11] C. F. Qiao, Phys. Lett. B **639**, 263 (2006).
[12] L. Maiani, V. Riquer, F. Piccinini, and A. D. Polosa, Phys. Rev. D **72**, 031502(R) (2005).
[13] X. Liu, X. Q. Zeng, and X. Q. Li, Phys. Rev. D **72**, 054023 (2005).
[14] E. S. Swanson, Phys. Rep. **429**, 243 (2006).
[15] B. Aubert *et al.* (*BABAR* Collaboration), Phys. Rev. D **76**, 111105 (2007).
[16] G. Pakhlova *et al.* (Belle Collaboration), Phys. Rev. D **77**, 011103 (2008).
[17] G. Pakhlova *et al.* (Belle Collaboration), Phys. Rev. Lett. **98**, 092001 (2007).
[18] J. Libby *et al.* (CLEO Collaboration), Nucl. Phys. B, Proc. Suppl. **181**, 127 (2008).
[19] B. Aubert *et al.* (*BABAR* Collaboration), Nucl. Instrum. Methods Phys. Res., Sect. A **479**, 1 (2002).
[20] S. Agostinelli *et al.* (GEANT Collaboration), Nucl. Instrum. Methods Phys. Res., Sect. A **506**, 250 (2003).
[21] M. Benayoun *et al.*, Mod. Phys. Lett. A **14**, 2605 (1999).
[22] E. Eichten, K. Gottfried, T. Kinoshita, K. D. Lane, and T. M. Yan, Phys. Rev. D **21**, 203 (1980).
[23] J. M. Blatt and W. F. Weisskopf, *Theoretical Nuclear Physics* (John Wiley & Sons, New York, 1952).
[24] F. Iddir, L. Semlala, arXiv:hep-ph/0611183.